RadioGraphics

Steady-State MR Imaging Sequences: Physics, Classification, and Clinical Applications[1]

Govind B. Chavhan, MD, DNB • Paul S. Babyn, MD • Bhavin G. Jankharia, MD • Hai-Ling M. Cheng, PhD • Manohar M. Shroff, MD

TEACHING POINTS
See last page

Steady-state sequences are a class of rapid magnetic resonance (MR) imaging techniques based on fast gradient-echo acquisitions in which both longitudinal magnetization (LM) and transverse magnetization (TM) are kept constant. Both LM and TM reach a nonzero steady state through the use of a repetition time that is shorter than the T2 relaxation time of tissue. When TM is maintained as multiple radiofrequency excitation pulses are applied, two types of signal are formed once steady state is reached: preexcitation signal (S–) from echo reformation; and postexcitation signal (S+), which consists of free induction decay. Depending on the signal sampled and used to form an image, steady-state sequences can be classified as *(a)* postexcitation refocused (only S+ is sampled), *(b)* preexcitation refocused (only S– is sampled), and *(c)* fully refocused (both S+ and S– are sampled) sequences. All tissues with a reasonably long T2 relaxation time will show additional signals due to various refocused echo paths. Steady-state sequences have revolutionized cardiac imaging and have become the standard for anatomic functional cardiac imaging and for the assessment of myocardial viability because of their good signal-to-noise ratio and contrast-to-noise ratio and increased speed of acquisition. They are also useful in abdominal and fetal imaging and hold promise for interventional MR imaging. Because steady-state sequences are now commonly used in MR imaging, radiologists will benefit from understanding the underlying physics, classification, and clinical applications of these sequences.

Abbreviations: CSF = cerebrospinal fluid, FID = free induction decay, GRE = gradient-echo, LM = longitudinal magnetization, RF = radiofrequency, SNR = signal-to-noise ratio, TE = echo time, TM = transverse magnetization, TR = repetition time, 3D = three-dimensional

RadioGraphics 2008; 28:1147–1160 • **Published online** 10.1148/rg.284075031 • **Content Codes:** MR PH

[1]From the Department of Diagnostic Imaging, Hospital for Sick Children and University of Toronto, 555 University Ave, Toronto, ON, Canada M5G 1X8 (G.B.C., P.S.B., H.L.M.C., M.M.S.); and Jankharia Imaging Center, Mumbai, India (B.G.J.). Presented as an education exhibit at the 2006 RSNA Annual Meeting. Received February 23, 2007; revision requested May 18; final revision received October 5; accepted October 24. All authors have no financial relationships to disclose. **Address correspondence to** G.B.C. (e-mail: *drgovindchavhan@yahoo.com*).

Introduction

With recent advances in gradient system and power amplifier technology leading to higher gradient amplitude and higher slew rates, gradient-echo (GRE) sequences have become fast and robust. One type of fast GRE sequence is a steady-state sequence, in which longitudinal magnetization (LM) and transverse magnetization (TM) are kept constant (ie, at the same magnitude) with each cycle (1,2). Steady-state sequences have proved useful in a variety of applications, including imaging of the heart and vessels. They are now commonly available for and frequently used in magnetic resonance (MR) imaging. Hence, it is imperative for radiologists to understand the basic physics and applications of these sequences.

In this article, we review the definition and the means of achieving steady state; discuss and illustrate various types of steady-state sequences and their clinical applications; describe nuances of GRE sequences and the nomenclature for steady-state sequences used by different vendors of MR imaging equipment; and discuss the advantages of steady-state sequences.

What Is Steady State?

When a patient is placed in a magnet (MR imager), randomly moving protons in the body align along the Z axis (the long axis of the patient as well as the bore in superconducting magnets) to form a magnetization force under the influence of an external magnetic field. This magnetization force is represented as a vector along the positive side of the Z axis and is called LM. When LM is tilted by a radiofrequency (RF) pulse into the transverse plane, it is called TM. The net magnetization is the sum of LM and TM. The magnitudes of LM and TM do not remain constant during one repetition time (TR) period or with subsequent excitations with conventional spin-echo sequences. Details concerning LM and TM and their behavior with pulse sequences can be found in standard MR imaging textbooks (3,4).

When the same sequence of RF excitations and relaxation is repeated, a steady state forms in which the magnetization at some point in the sequence is constant from one repetition to the next. This article focuses specifically on the scenario in which both LM and TM reach a nonzero steady-state condition (ie, as used in steady-state sequences).

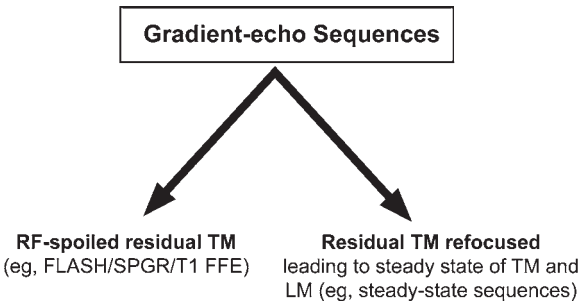

Figure 1. Chart illustrates the two types of GRE sequences. *FLASH* = fast low-angle shot (Siemens Medical Systems, Erlangen, Germany), *SPGR* = spoiled gradient-recalled echo (GE Medical Systems, Milwaukee, Wis), *FFE* = fast field echo (Philips Medical Systems, Best, the Netherlands).

There are basically two types of fast GRE sequences (Fig 1). In the first type, residual TM is spoiled; thus, the sequence is called an incoherent or spoiled GRE sequence. Examples of this type include FLASH (Siemens), SPGR (GE Medical Systems), and T1-FFE (Philips) sequences. In the second type of fast GRE sequence, TM is not spoiled but is refocused to contribute to steady-state formation. This type of sequence is called a coherent or steady-state GRE sequence. Note that although a GRE sequence with spoiled TM is not considered a classic steady-state sequence, steady state is achieved for the LM component. For this reason, these sequences have been called steady-state incoherent sequences by some authors (5). Classic steady-state sequences have been termed steady-state coherent sequences by these same authors (5).

Teaching Point

How Is Steady State Achieved?

A steady state of both LM and TM is achieved by keeping the TR shorter than the T2 relaxation times of the tissue (6). Because the TR is shorter than T2, there is not enough time for TM to decay completely before the next RF pulse excitation, so that there will be some residual TM left over. This residual TM is fed back into LM with the next RF excitation. At the same time, a portion of LM is flipped into the transverse plane. If this sequence is continued, after several TR periods a steady state of the magnetization is established, with constant magnitudes of LM and TM (Fig 2). The amount of TM fed back into LM increases with the flip angle up to 90°. Therefore, the degree of steady-state equilibrium increases with flip angle (6). The usual range of flip angle required to achieve the highest signal in

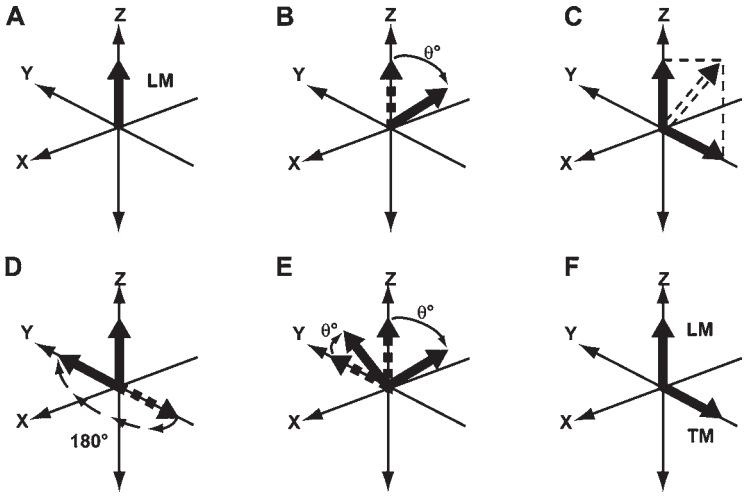

Figure 2. Graphs show steady-state formation in GRE pulse sequences. In *A*, magnetization before application of an RF excitation pulse is shown. In *B*, the RF pulse tips the magnetization by θ°. In *C*, the resulting tipped magnetization has an LM that recovers and a TM that decays during the TR period. As seen in *D*, during the TR period, the TM can precess through a 180° phase shift in the transverse plane. In *E*, the succeeding RF pulse simultaneously tips a component of residual TM back along the +Z axis and a portion of LM into the transverse plane. In *F*, after several TR periods, this feeding of LM into TM and vice versa establishes a steady state of both LM and TM.

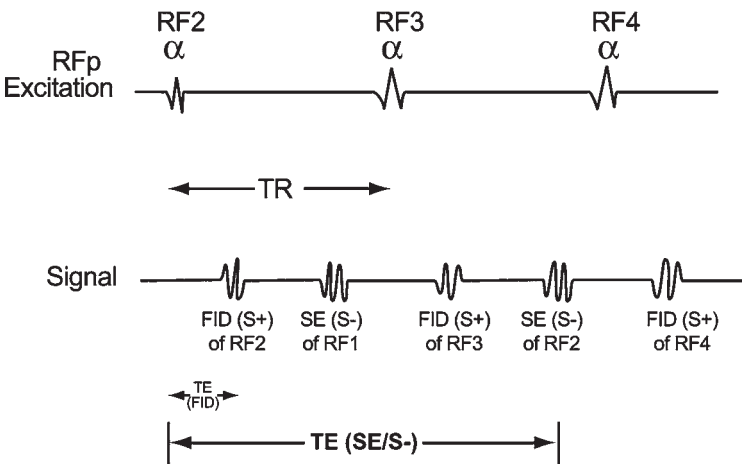

Figure 3. Signals produced in steady state. Once the steady equilibrium of LM and TM is reached, two types of signals are produced: The first signal is free induction decay (FID) (S+), which is formed after excitation with the most recent RF pulse. The second component is spin echo (*SE* [S–]), which is formed when residual echo from the previous RF excitation is refocused by the current RF pulse. α = flip angle.

a steady state is 50°–80° (7). As echo time (TE) is increased, T2* weighting of the sequence increases (6).

Reaching Steady State

The transient phase that precedes steady-state magnetization is complex and oscillatory and requires several TR periods. When an α/2 pulse (where α = flip angle) is sent at a time TR/2 before a train of RF pulses, steady state is reached in approximately 40–50 RF pulses (8). With on-resonance frequency, an RF pulse of α/2 sent before a train of RF pulses forces the magnetization vector immediately into steady state (9). For off-resonance spins, however, signal oscillations persist despite the α/2 pulse. This situation can be improved with the application of linearly increasing flip angles, allowing a steady state of magnetization to be reached in 10–15 pulses (10,11). With linear flip angle preparation, fluctuations are reduced and data can be acquired in the transient phase (9). Once steady state is reached, the magnetization vector oscillates between +α/2 and –α/2 about the Z axis (9).

Types of Steady-State Sequences

When phase-coherent RF pulses of the same flip angle are applied with a constant TR that is shorter than the T2 of the tissue, a dynamic equilibrium is achieved between TM and LM (12). Once this equilibrium is reached, two types of signals are produced (Fig 3) (12). The first type is a postexcitation signal (S+) that consists of FID arising from the most recent RF pulse. The second signal is echo reformation that occurs prior to excitation (S–) and results when residual echo is refocused at the time of the subsequent RF pulse. FID (S+) has mixed T1 and T2* weighting. The spin echo (S–) is strongly T2 weighted and has negligible T2* weighting (13,14).

Teaching Point

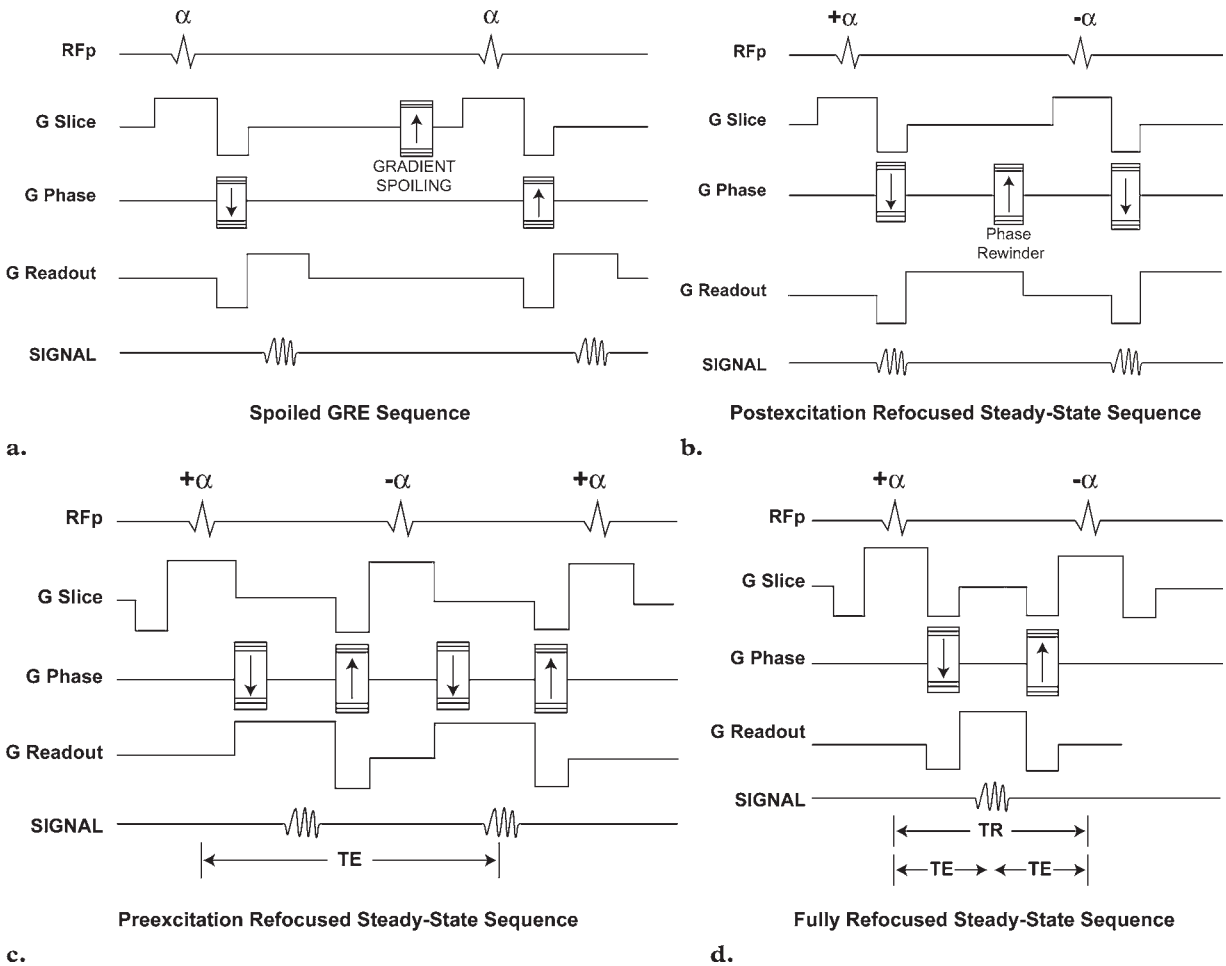

Figure 4. GRE sequences. α = flip angle, *G* = gradient. **(a)** Spoiled GRE sequence. After the signal is acquired with reversal of the frequency-encoding (readout) gradient, residual TM is dephased with a spoiler gradient so that it does not interfere with the next RF excitation. **(b)** Postexcitation refocused steady-state sequence. With this sequence, instead of spoiling, residual TM is refocused with a gradient along the phase-encoding axis (phase rewinder) such that a steady state of TM is achieved after a few TR periods. The difference in contrast between this sequence and a spoiled GRE sequence (cf **a**) is manifested only when TR is less than T2 and large flip angles are used. Slice-selection and readout gradients are not balanced. **(c)** Preexcitation refocused steady-state sequence. Time reversal of both slice-selection and readout gradients (cf **b**) is done in this sequence. which consequently is called "reversed FISP" by Siemens. As with a postexcitation refocused steady-state sequence, slice-selection and readout gradients are not balanced. TE is longer than TR, since the signal of the current RF excitation is refocused at the time of the subsequent excitation. **(d)** Fully refocused steady-state sequence. Gradients along all three axes (slice-selection, phase-encoding, and readout) are fully balanced such that, between RF pulses, the sum of positive gradient areas is exactly balanced by the sum of negative gradient areas. Because there is no dephasing of the magnetization within the TR period, it is nearly identical at the beginning and at the end of the period (just before the next RF excitation).

Teaching Point

Depending on what signals are sampled and used for image formation, steady-state sequences can be classified as follows (Fig 4, Table 1) (1,15):

1. Postexcitation refocused steady-state sequences, in which only the FID (S+) component is sampled (eg, FISP [Siemens], GRASS [GE Medical Systems], FFE, Fourier-acquired steady-state technique [FAST; Picker International, Cleveland, Ohio]).

2. Preexcitation refocused steady-state sequences, in which only the spin-echo (S–) component is used for image formation (eg, PSIF [reversed FISP, Siemens]; steady-state free precession [SSFP, GE Medical Systems]; T2-FFE).

3. Fully refocused steady-state sequences, in which both FID (S+) and spin-echo (S–) components are used for image formation. This sequence is also called balanced SSFP, since gradients applied in all three axes are balanced (eg, true FISP, FIESTA [GE Medical Systems], balanced FFE).

Table 1
Features of Major GRE Sequences

Features	Steady-State Sequences			
	Spoiled GRE Sequence	Postexcitation Refocused	Preexcitation Refocused	Fully Refocused
Signal used for image formation	FID	FID (S+)	Spin echo (S–)	S+, S–
Refocusing axis	. . .	Phase-encoding	Phase-encoding	Slice-selection, phase-encoding, frequency-encoding
Image weighting	T1	T2*	T2	Both T1 and T2 (determined by T2/T1 ratio of tissue)
Appearance of vessels	Bright	Dark	Dark	Bright on two-dimensional images, dark on 3D images
Motion sensitivity	Sensitive	Sensitive due to long TE and acquisition window	Sensitive due to long effective TE and "crusher" gradient	Intrinsically motion insensitive
Artifacts	Susceptibility	Movement, flow, susceptibility	Movement, flow	Banding artifacts
Advantages	Fast T1-weighted images can be acquired before and after injection of gadolinium-based contrast material	T2*-weighted images can be obtained	True T2-weighted images can be obtained	High SNR, less sensitive to motion
Major applications	Pre- and postcontrast T1-weighted images of various body parts, dynamic acquisitions with multiple phases during contrast material injection, MR angiography	Cartilage and meniscal evaluation, MR angiography; now largely replaced by fully balanced steady-state sequences	Cerebrospinal fluid (CSF) flow studies, inner ear, CSF fistulas, interventional MR imaging, diffusion MR imaging, MR myelography	Cardiac imaging, abdominal imaging, fetal imaging

Apart from these basic types of steady-state sequences, a few other commonly used steady-state sequences can be formed by modifying the fully refocused steady-state sequences.

Constructive Interference into Steady State/FIESTA-C

Constructive interference into steady state (CISS, Siemens)/FIESTA-C (1,16) is a slow version of fully refocused steady-state sequences with a TR of approximately 15–20 msec. CISS combines two consecutive runs of three-dimensional (3D) balanced SSFP. The first run makes use of alternating $+\alpha$ and $-\alpha$ excitation pulses (where α = flip angle), and the second run is performed with constant α pulses. The two image sets thus acquired show mutually shifted "banding artifacts." Maximum intensity projection between these two data sets yields the banding artifact–free CISS image (7).

Dual-Echo Steady-State Sequence

The dual-echo steady-state (DESS, Siemens) sequence (1) is a variation of true FISP. In the DESS sequence, images are formed from FISP (S+) and PSIF (S–) signals separately and are then combined to form a single image. In the true FISP sequence, the two signals (S+ and S–)

themselves are combined to form an image. PSIF signal accentuates the signal intensity of structures or components in the image with long T2, such as fluid. Because of its T1 weighting, FISP (S+) signal provides anatomic details (9).

Steady-State Projection Imaging with Dynamic Echo Train Readout

Steady-state projection imaging with dynamic echo train readout (SPIDER, Siemens) (13,17) is a modification of the true FISP sequence in which k space is filled with radial trajectory. There is no phase-encoding gradient. The direction of the readout gradient is rotated in a series of projections like the spokes of a wheel (18). For each measurement, the gradient amplitudes are varied to provide another projection (13). Multiple echoes are acquired following each RF excitation while refocusing the magnetization to maintain a steady state (19).

Nuances of GRE Sequences

Differences between various steady-state sequences, including spoiled GRE sequences, lie in the differences in gradient switching patterns applied between consecutive excitation pulses. Different gradient time courses produce different dephasing within TR that leads to different contrast among the various types of steady-state sequences (7).

In spoiled GRE sequences (Figs 4a, 5a), residual TM is dephased by a spoiler gradient after the signal has been read and before the next excitation pulse is sent. In postexcitation refocused steady-state sequences (Figs 4b, 5b), residual TM is refocused with an extra phase-encoding gradient with opposite polarity. FID is acquired in both types of sequences, but the FID in postexcitation refocused steady-state sequences has contributions from various refocused echoes such as spin echoes and stimulated echoes (transverse coherence) (20). Differences in contrast behavior between these two sequences are manifested only when TR is less than T2 and a large flip angle is used (8). For the short TR, spoiled GRE sequences display T1 weighting, whereas postexcitation refocused steady-state sequences yield T2/T1–weighted images with sensitivity to T2* effects.

On the other hand, in preexcitation refocused steady-state sequences (Figs 4c, 5c), time reversal of both slice-selection and readout gradients is performed to acquire the PSIF (S–) signal. This signal represents a complicated overlap of spin echoes and stimulated echoes. Effective TE is greater than TR, since the signal of the current RF excitation is refocused in the next excitation. PSIF (S–) signal has the same sensitivity to inhomogeneity and susceptibility as the FID of spoiled GRE sequences and the FISP (S+) signal of postexcitation refocused steady-state sequences. Images produced with preexcitation steady-state sequences are heavily T2 weighted. Contrast is highly dependent on the flip angle.

Teaching Point

The main difference between fully refocused steady-state sequences (balanced SSFP) (Fig 4d) and other GRE sequences is the use of balanced gradients in all three axes (slice-selection, phase-encoding, and readout) such that gradient-induced dephasing within TR is exactly zero (21). This makes balanced SSFP relatively insensitive to motion. In nonbalanced GRE sequences, slice-selection and readout gradients are not balanced. Contrast in balanced SSFP depends on the T2/T1 ratio. Thus, there is very high signal intensity for fat and water because of their high T2/T1 ratio. Balanced SSFP is not as sensitive to conventional T2* effects as are other GRE sequences (Fig 5d). This phenomenon may be related to field inhomogeneity–induced dephasing being (within a certain range) nearly completely refocused at TE = TR/2, leading to the formation of a spin echo rather than a gradient echo (22).

Contrast differences also exist between two-dimensional and 3D balanced SSFP sequences because of the long duration of the transient phase (7). Two-dimensional balanced SSFP images display contrast between proton density and T2/T1, whereas 3D images have pure steady-state contrast characterized by poor gray matter–white matter differentiation and increased signal from fat and water. Whereas vessels are bright due to flow enhancement on two-dimensional images, they are dark on 3D balanced SSFP images (7). Vessels are bright with spoiled GRE sequences, whereas they are dark with pre- and postexcitation refocused steady-state sequences because of the sensitivity of these sequences to the flow resulting from dephasing of TM (Fig 5).

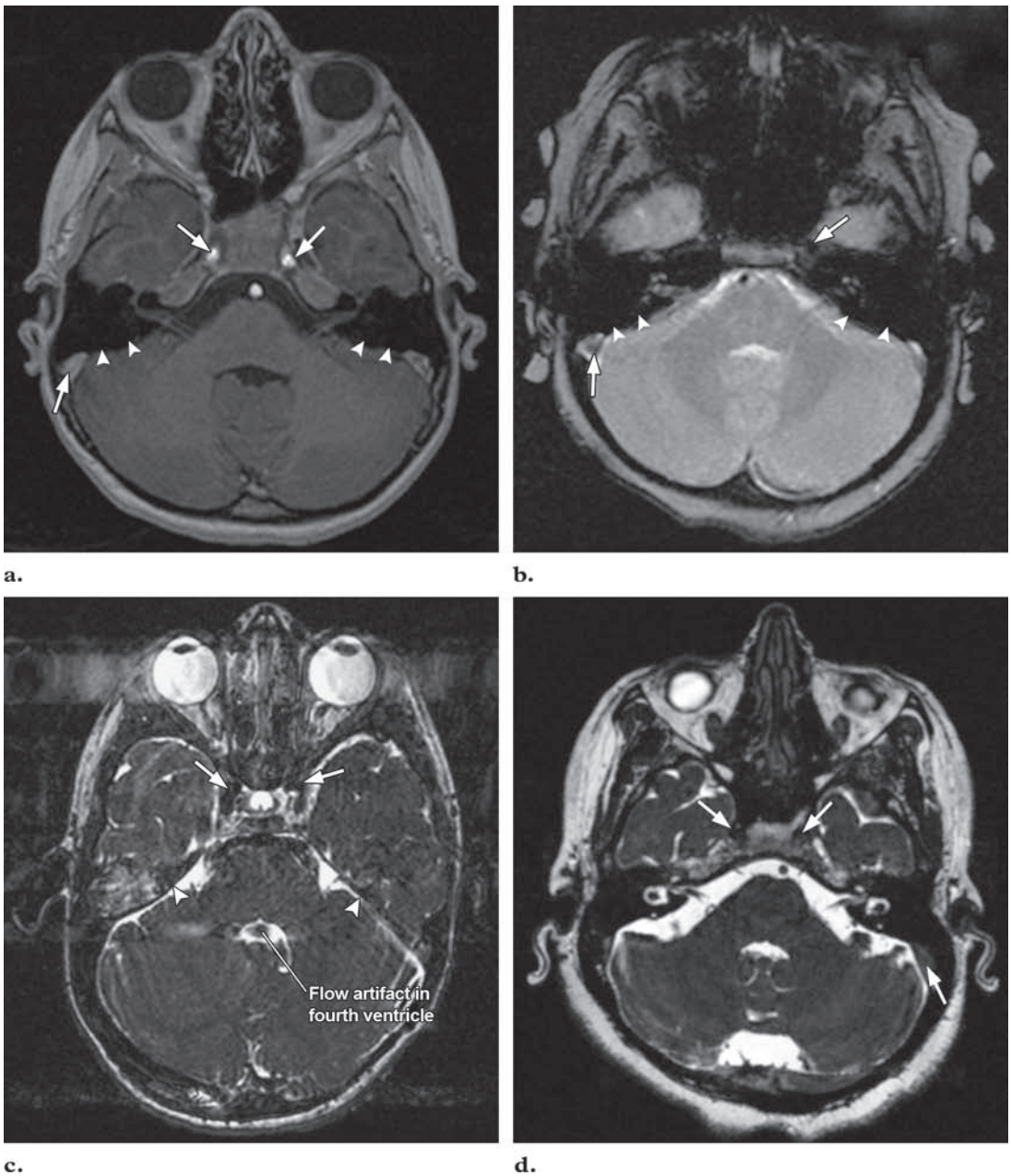

Figure 5. Nuances of GRE sequences. **(a)** On an axial 3D SPGR (spoiled GRE) image obtained after the intravenous injection of gadolinium-based contrast material, the CSF is dark. Gray matter–white matter differentiation is seen in the cerebellum and the temporal lobes. Vessels are bright (arrows) and were in fact bright even on noncontrast images from this sequence. No significant susceptibility artifacts are seen at tissue interfaces (arrowheads). **(b)** On an axial fast MPGR (GE Medical Systems) image (postexcitation refocused steady-state sequence), the CSF is bright and vessels are dark (arrows). Gray matter–white matter differentiation is seen. Note the marked susceptibility artifacts at tissue interfaces (arrowheads) owing to the T2* weighting of the sequence. **(c)** On an axial 3D PSIF image (preexcitation refocused steady-state sequence), the CSF is markedly bright and vessels are dark (arrows). Gray matter–white matter differentiation is not possible. No significant susceptibility artifacts are seen at tissue interfaces (arrowheads). However, marked sensitivity to flow and motion is seen, with CSF flow artifact in the fourth ventricle. **(d)** On an axial 3D CISS image (modified fully refocused steady-state sequence), the CSF is bright but vessels (arrows) are not. Gray matter–white matter differentiation is not possible. No significant susceptibility, motion, or flow artifacts are seen.

Table 2
Manufacturers' Nomenclature for Major GRE Sequences

	Type of Sequence			
Manufacturer	Spoiled GRE	Postexcitation Refocused*	Preexcitation Refocused*	Fully Refocused*
Siemens	FLASH	FISP	PSIF (reversed FISP)	True FISP
GE Medical Systems	SPGR, MPGR	GRASS, fast MPGR	SSFP	FIESTA
Philips	T1-FFE	FFE	T2-FFE	Balanced FFE

Sources.—References 1, 13, and 15.
Note.—FFE = fast field echo, FIESTA = fast imaging employing steady-state acquisition, FISP = fast imaging with steady-state precession, FLASH = fast low-angle shot, GRASS = gradient-recalled acquisition in the steady state, MPGR = multiplanar gradient-recalled, SPGR = spoiled gradient-recalled, SSFP = steady-state free precession.
*Steady-state sequence.

Nomenclature among Different Vendors

There is much confusion regarding the nomenclature for sequences used by different MR imaging equipment manufacturers. This holds true for steady-state sequences as well. Some authors classify whole groups of steady-state sequences as SSFP sequences (2,12,23), whereas GE Medical Systems reserves this label only for preexcitation refocused steady-state sequences. Fully refocused steady-state sequences are also called balanced SSFP sequences (7). The nomenclature used by major manufacturers like Siemens, GE Medical Systems, and Philips is shown in Table 2.

What Are the Advantages of Steady-State Sequences?

Shorter TR and therefore shorter imaging times can be achieved with steady-state sequences. With short TR and TE, all tissues with reasonably long T2 relaxation times will demonstrate additional signal due to various refocused echo paths (13). The advantages of steady-state sequences include the highest possible signal-to-noise ratio (SNR) per unit time among all known sequences (7), better contrast-to-noise ratio compared with spoiled GRE sequences, and increased signals, along with improved speed of acquisition. The speed of acquisition is comparable to that of fast spin-echo and echoplanar imaging sequences. It is possible to study rapid physiologic processes with breath-hold acquisitions. Steady-state sequences have the advantage of speed that reduces motion artifacts from (for example) respiration and peristalsis.

Clinical Applications

Postexcitation Refocused Steady-State Sequences

Postexcitation refocused steady-state sequences are most often used to generate T2*-weighted images, depending on the TR and flip angle chosen. They have been used to detect brain hemorrhages and to evaluate cartilage and meniscal lesions (Fig 6), as well as for MR angiography (1).

These sequences cannot make use of a high bandwidth and are therefore associated with an increased acquisition window and a relatively long TE compared with balanced SSFP sequences. They are also sensitive to motion and flow. These features have reduced the number of clinical applications of these sequences, which have been taken over by fully refocused steady-state sequences.

Preexcitation Refocused Steady-State Sequences

A preexcitation refocused steady-state sequence makes use of spin-echo (S–) signal. FID (S+) is destroyed by a crusher gradient (a gradient that dephases all signals but rephases only those that are generated by the correct pulses) on the

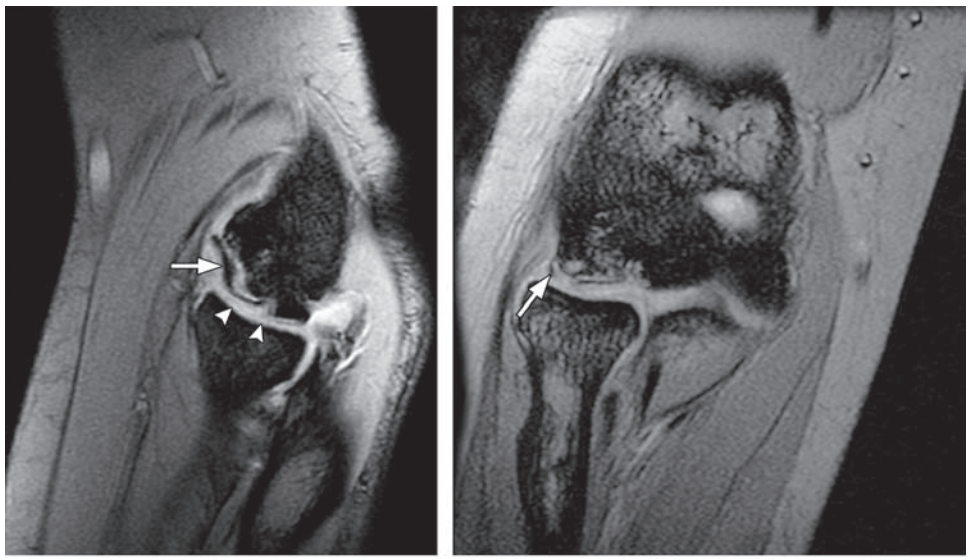

a. b.

Figure 6. Joint imaging with a fast MPGR sequence in a 14-year-old girl who was undergoing steroid treatment for systemic lupus erythematosus. On sagittal **(a)** and coronal **(b)** fast MPGR images (postexcitation refocused steady-state sequence) of the elbow, changes of avascular necrosis are seen, with a large osteochondral defect (arrow) in the anterior part of the capitellum. Articular cartilage is seen as a bright structure surrounding the articular surface of bones (arrowheads in **a**).

slice-selection axis. It is heavily T2 weighted and has negligible T2* weighting (Fig 5c) (13). Its long effective TE and crusher gradient increase sensitivity to motion and flow, thereby limiting its clinical use (23). Nonetheless, it has proved useful for evaluation of various conditions. It has been used to differentiate an intracranial cyst from a CSF space (14). A cine-mode retrospectively electrocardiographically gated flow-sensitive PSIF sequence shows signal attenuation in CSF spaces due to CSF flow, whereas persistent increased T2 signals are seen in cystic spaces or cysts not communicating with CSF spaces. PSIF is also useful for the detection of CSF fistulas (24), CSF flow studies for the evaluation of third ventriculostomy (25), MR myelography (26), and diffusion imaging of the spine to differentiate between osteoporotic and neoplastic fractures (27). In addition, it has been used to visualize tumor and thermal lesions during intervention (13) and for other interventions (28,29).

Fully Refocused Steady-State Sequences

Fully refocused steady-state sequences have introduced a new era in MR imaging and have revolutionized cardiac imaging. All three axes are balanced in this type of sequence, which is the least sensitive to motion artifacts. However, the sequence is somewhat limited by banding artifacts (linear bands of low signal), especially at air-tissue interfaces caused by field inhomogeneities (18,30). Banding artifacts can be reduced by alternating the phase of the RF pulse by 180° with subsequent TR periods, by keeping TR as low as possible, and by using the proper shimming (9). Present and potential clinical applications of balanced SSFP are discussed in the following paragraphs.

Cardiac Imaging.—Contrast in balanced SSFP is dependent on the T2/T1 ratio. Blood has a much higher T2/T1 ratio than does myocardium. The sequence is flow compensated and intrinsically insensitive to flow because of even echo rephasing, which is due to the multiple GRE pulses used. An intrinsically high SNR makes it possible to image with a higher bandwidth and a very short TR. All of these factors make this sequence suitable for cardiac imaging (Fig 7) (2), wherein it is used to assess myocardial viability (Fig 8), perfusion, pericardial diseases, and congenital heart diseases (Fig 9). Cine true FISP is used to assess cardiac wall motion, cardiac function, and cardiac valves (Fig 10). Coronary assessment with true FISP is not yet clinically useful because of the poor resolution of distal coronary arteries and branches. However, true FISP does hold promise in coronary imaging (31,32).

Teaching Point

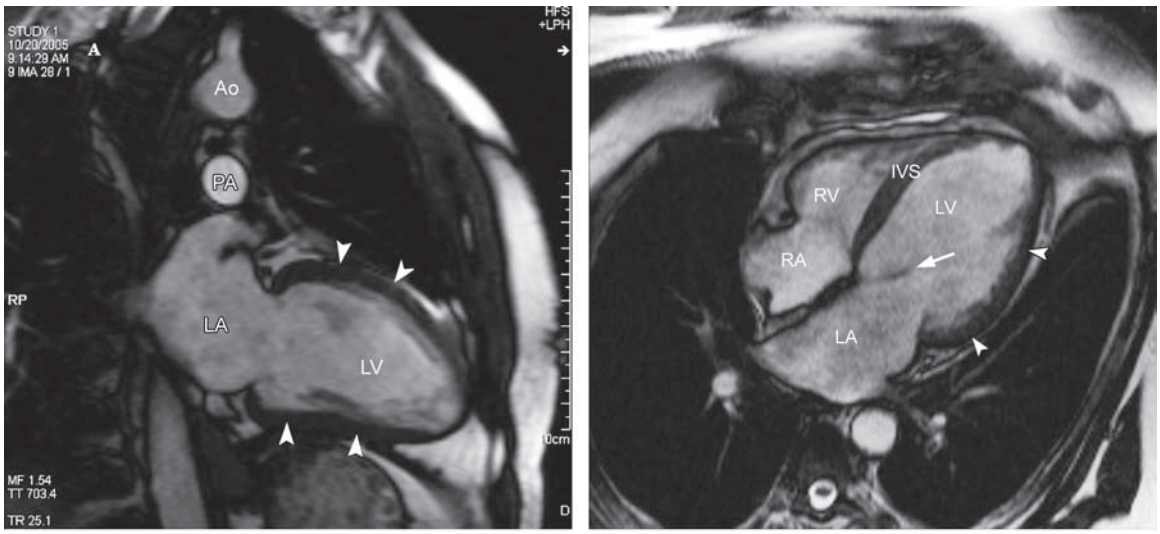

a. b.

Figure 7. Cardiac imaging with a true FISP sequence. True FISP images (two-chamber [**a**] and four-chamber [**b**] views) show the normal cardiac anatomy. Dark myocardium (arrowheads) and valve leaflets (arrow in **b**) are well appreciated against a background of bright blood. *Ao* = aorta, *IVS* = interventricular septum, *LA* = left atrium, *LV* = left ventricle, *PA* = pulmonary artery, *RA* = right atrium, *RV* = right ventricle.

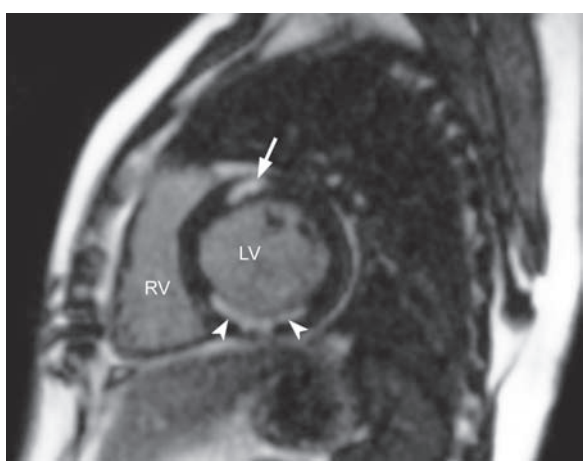

Figure 8. Assessment of myocardial viability. True FISP image (short-axis view) obtained 10 minutes after contrast material injection shows delayed enhancement in the anteroseptal (arrow) and inferoseptal (arrowheads) left ventricular wall, findings that are suggestive of nonviable myocardium. Because bright areas represent nonviable myocardium, it is said that "bright is dead" at viability imaging. Cardiac MR imaging has arguably become the new standard for the assessment of myocardial viability and scar. *LV* = left ventricle, *RV* = right ventricle.

Abdominal Imaging.—The entire abdomen can be imaged with balanced SSFP during a single breath hold. Blood, bile, and fat are bright on true FISP images due to their high T2/T1 ratio (Fig 11). Bile ducts and pancreatic ducts are well seen with this sequence (33). Blood vessels can be assessed without contrast material injection (33). This sequence is especially useful in patients who have difficulty holding their breath. It has also proved useful in *(a)* the delineation of bowel wall disease and overall bowel anatomy when performed with a water-based intraluminal distending agent (34), and *(b)* the evaluation of renal and pelvic disease.

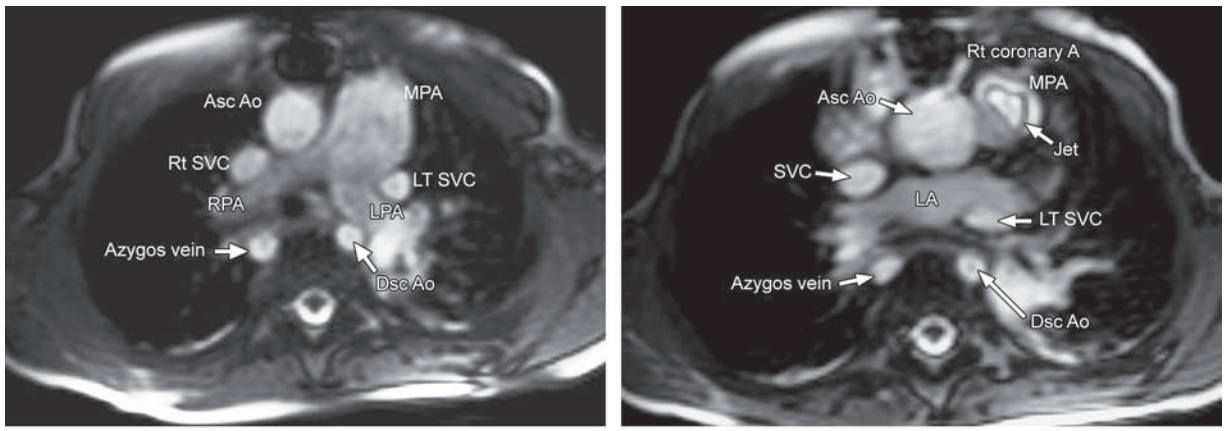

a. b.

Figure 9. Congenital heart disease in a 3-year-old boy. Axial FIESTA images obtained at the supracarinal **(a)** and carinal **(b)** levels show the left superior vena cava *(SVC)* opening into the coronary sinus. The patient also had interruption of the suprarenal inferior vena cava with azygous continuation. Pulmonary stenosis is seen as a bright jet in the main pulmonary artery *(MPA)*. *A* = artery, *Asc Ao* = ascending aorta, *Dsc Ao* = descending aorta, *LA* = left atrium, *LPA* = left pulmonary artery, *RPA* = right pulmonary artery.

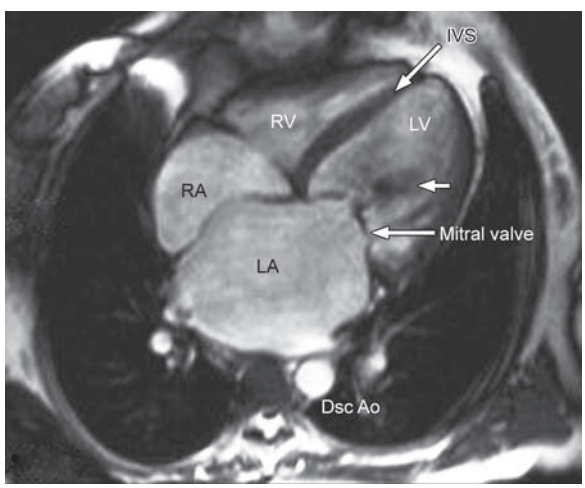

Figure 10. Cardiac valvular disease. True FISP image (four-chamber view) shows stenosis of the mitral valve with a jet (arrow) in the left ventricle *(LV)*. The left atrium *(LA)* is dilated. *Dsc Ao* = descending aorta, *IVS* = interventricular septum, *RA* = right atrium, *RV* = right ventricle.

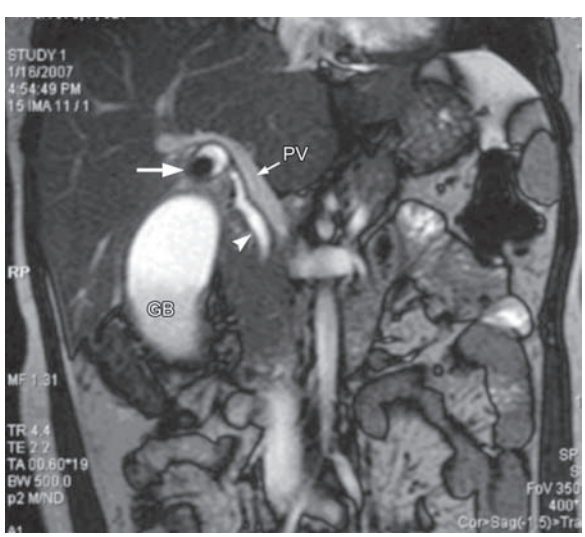

Figure 11. Abdominal imaging with a balanced SSFP sequence. On a coronal true FISP image of the abdomen, the vessels and biliary system are bright. Note the calculus (arrow) in the neck of the distended gallbladder *(GB)*, with prominence of the common bile duct (arrowhead) lateral to the portal vein *(PV)*. Note also the movement artifact–free definition of the abdominal organs.

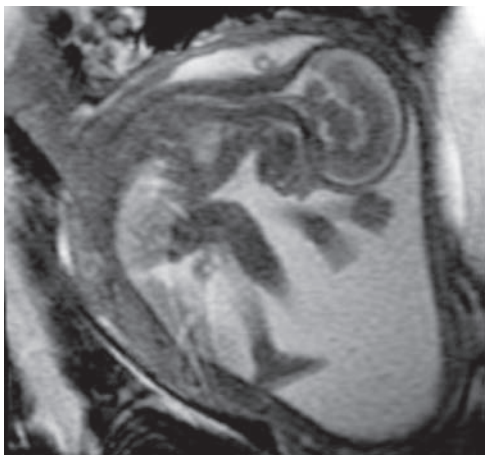

Figure 12. Fetal MR imaging with a FIESTA sequence. Static image shows a fetus in a sagittal orientation. Cine FIESTA sequences of the gravid uterus are used to study fetal movements.

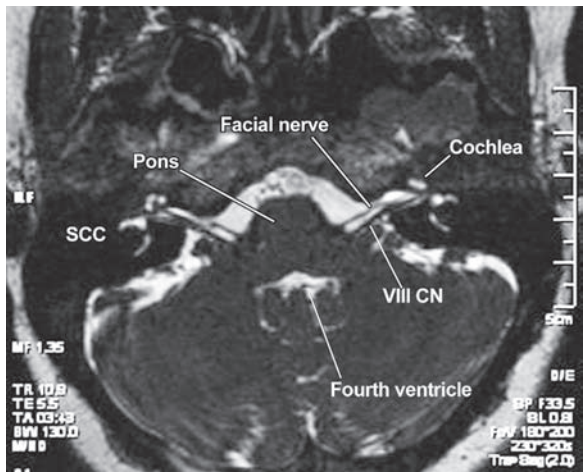

Figure 13. Cranial nerve imaging with CISS. Axial CISS image of the posterior cranial fossa shows a normal facial nerve and eighth cranial nerve *(VIII CN)* and internal ear structures such as the cochlea and lateral semicircular canal *(SCC)*.

Fetal Imaging.—The speed of balanced SSFP and its high SNR have made it useful in fetal MR imaging (Fig 12). This sequence is useful for whole-body fetal imaging and has significantly lower RF absorption than do fast spin-echo sequences such as half-Fourier single-shot turbo spin-echo (HASTE, Siemens) or single-shot fast spin-echo (SSFSE, GE Medical Systems) sequences. Some authors have found it to be a safer and more effective alternative in evaluating the fetal brain (35).

Interventional MR Imaging.—True FISP at low-field-strength MR imaging can be useful for needle path guidance (29).

Modified Fully Refocused Steady-State Sequences

CISS/FIESTA-C.—CISS/FIESTA-C has become a sequence of choice for evaluating the cranial nerves. It shows dark cranial nerves against a background of bright CSF. Cerebellopontine angle cistern lesions and cranial nerves VII and VIII in the internal auditory canal and labyrinth are best evaluated with CISS (Figs 13, 14) (16). It is also used in the evaluation of spinal diseases such as intra- and extraaxial cystic abnormalities, dysraphic malformations, and disturbances of CSF

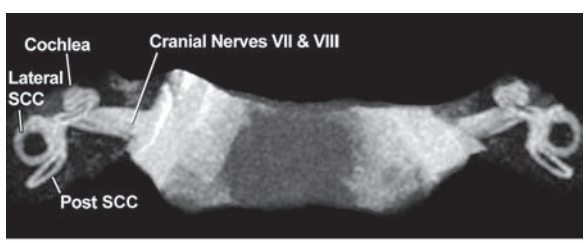

a.

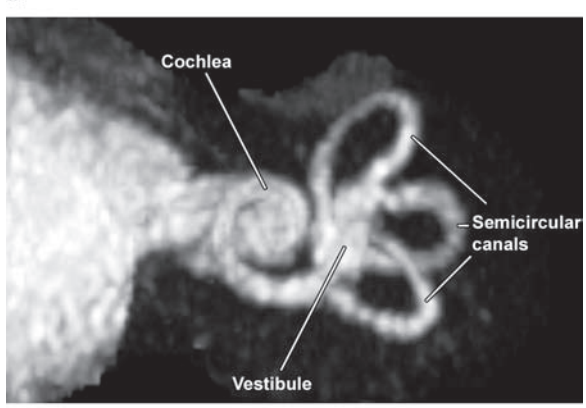

b.

Figure 14. Internal ear imaging with a 3D FIESTA-C sequence. Bilateral **(a)** and left-sided **(b)** maximum-intensity-projection images from 3D FIESTA-C data show the normal vestibule and cochlea. *Post* = posterior, *SCC* = semicircular canal.

circulation (36). Other uses of CISS include detection of neurovascular compression in patients with trigeminal neuralgia (37), evaluation of cavernous malformation of the brainstem (38) or of

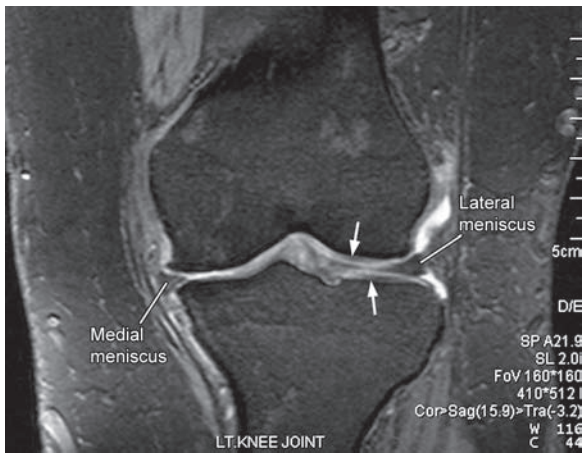

Figure 15. Articular cartilage imaging with DESS in a 49-year-old woman with early signs of osteoarthritis. On this coronal DESS image of the left knee joint, articular cartilage is seen as an intermediate-signal-intensity line covering articular surfaces of bone in the lateral compartment (arrows). Note the loss of articular cartilage with reduction in the joint space in the medial compartment.

root avulsions in brachial plexus injury resulting from birth trauma (39), and MR cisternographic evaluation of CSF rhinorrhea (40).

DESS.—DESS with water excitation pulses (slice-selective composite pulses that excite only water spins while lipid spins are left in equilibrium, thereby producing no signal) is the sequence of choice for the evaluation of articular cartilage (Fig 15) (41). It is also useful in the evaluation of unossified epiphyseal cartilage in children.

SPIDER.—SPIDER is useful in real-time interactive cardiac imaging (13,17,19) and fast tracking of interventional devices (13).

Conclusions

Steady-state sequences are fast GRE sequences in which residual TM is refocused, leading to a constant magnitude for LM and TM during acquisition. Very high SNR and contrast-to-noise ratio and fast acquisitions make steady-state sequences suitable for imaging rapid physiologic processes during a single breath hold. Steady-state sequences have had a significant impact on MR imaging in various body systems. They have revolutionized cardiac, abdominal, and fetal MR imaging and hold promise for interventional MR imaging.

References

1. Nitz WR. MR imaging: acronyms and clinical applications. Eur Radiol 1999;9:979–997.
2. Fuchs F, Laub G, Othomo K. TrueFISP: technical considerations and cardiovascular applications. Eur J Radiol 2003;46:28–32.
3. Mugler JP III. Basic principles. In: Edelman RR, Hesselink JR, Zlatkin MB, Crues JV, eds. Clinical magnetic resonance imaging. 3rd ed. Philadelphia, Pa: Saunders Elsevier, 2006;23–57.
4. Wood ML, Wehrli FW. Principles of magnetic resonance imaging. In: Stark DD, Bradley WG, eds. Magnetic resonance imaging. 3rd ed. St. Louis, Mo: Mosby,1999;1–14.
5. Haacke EM, Tkach JA. Fast MR imaging: techniques and clinical applications. AJR Am J Roentgenol 1990;155:951–964.
6. Hendrick RE. Image contrast and noise. In: Stark DD, Bradley WG, eds. Magnetic resonance imaging. 3rd ed. St Louis, Mo: Mosby, 1999; 43–68.
7. Scheffler K, Lehnhardt S. Principles and applications of balanced SSFP technique. Eur Radiol 2003;13:2409–2418.
8. Carroll TJ, Sakaie KE, Wielopolski PA, Edelman RR. Advanced imaging techniques, including fast imaging. In: Edelman RR, Hesselink JR, Zlatkin MB, Crues JV, eds. Clinical magnetic resonance imaging. 3rd ed. Philadelphia, Pa: Saunders Elsevier, 2006;187–230.
9. Finn JP, Deshpande VS, Simonetti OP. Pulse sequence design. In: Edelman RR, Hesselink JR, Zlatkin MB, Crues JV, eds. Clinical magnetic resonance imaging. 3rd ed. Philadelphia, Pa: Saunders Elsevier, 2006;137–173.
10. Nishimura DG, Vasanawala S. Analysis and reduction of the transient response in SSFP imaging [abstr]. In: Proceedings of the Eighth Meeting of the International Society for Magnetic Resonance in Medicine. Berkeley, Calif: International Society for Magnetic Resonance in Medicine, 2000; 301.
11. Deshpande VS, Chung YC, Zhang Q, et al. Reduction of transient signal oscillations in true FISP using a linear flip angle magnetization preparation. Magn Reson Med 2003;49:151–157.
12. Gyngell ML. The application of steady-state free precession in rapid 2DFT NMR imaging: FAST and CE-FAST sequences. Magn Reson Imaging 1988;6:415–419.
13. Nitz WR. Fast and ultrafast non-echo-planar MRI techniques. Eur Radiol 2002;12:2866–2882.
14. Hoffmann KT, Hosten N, Meyer BU, et al. CSF flow studies of intracranial cysts and cyst-like lesions achieved using reversed fast imaging with steady-state precession MR sequences. AJNR Am J Neuroradiol 2000;21:493–502.
15. Brown MA, Semelka RC. MR imaging abbreviations, definitions, and descriptions: a review. Radiology 1999;213:647–662.
16. Lane JI, Ward H, Witte RJ, et al. 3T imaging of cochlear nerve and labyrinth in cochlear-implant

candidates: 3D fast recovery fast spin-echo versus 3D constructive interference in steady-state techniques. AJNR Am J Neuroradiol 2004;25:618–622.
17. Boll DT, Merkle EM, Seamann DM, et al. Comparison of ECG-gated rectilinear versus real-time radial k-space sampling schemes in cine true FISP cardiac MRI. J Cardiovasc Magn Reson 2004;6(4):793–802.
18. Finn JP, Nael K, Deshpande V, Ratib O, Laub G. Cardiac MR imaging: state of the technology. Radiology 2006;241:338–352.
19. Larson AC, Simonetti OP. Real-time cardiac cine imaging with SPIDER: steady-state projection imaging with dynamic echo-train readout. Magn Reson Med 2001;46:1059–1066.
20. Frahm J, Haenicke W. Rapid scan techniques. In: Stark DD, Bradley WG, eds. Magnetic resonance imaging. 3rd ed. St Louis, Mo: Mosby, 1999; 87–124.
21. Oppelt A, Graumann R, Barfuss H, Fischer H, Hartl W, Schajor W. FISP: a new fast MRI sequence. Electromedica (Engl Ed) 1986;54:15–18.
22. Scheffler K, Henning J. Is true FISP a spin-echo or gradient-echo sequence? Magn Reson Med 2003; 49:395–397.
23. Tien RD, Bernstein M, MacFall J. Pulsatile motion artifact reduction in 3D steady-state-free-precession-echo brain imaging. Magn Reson Imaging 1993;11:175–181.
24. Eberhardt KE, Hollenbach HP, Deimling M, Tomandl BF, Huk WJ. MR cisternography: a new method for diagnosis of CSF fistulae. Eur Radiol 1997;7(9):1485–1491.
25. Hoffmann KT, Lehmann TN, Baumann C, Felix R. CSF flow imaging in management of third ventriculostomy with a reversed fast imaging with steady-state precession sequence. Eur Radiol 2003; 13(6):1432–1437.
26. Schnarkowski P, Wallner B, Goldmann A, Friedrich JM. MR-myelography of the lumbar spine using a PSIF sequence: first experiences. Aktuelle Radiol 1993;3(1):53–56.
27. Baur A, Huber A, Durr HR, et al. Differentiation of benign osteoporotic and neoplastic vertebral compression fractures with a diffusion-weighted, steady-state free precession sequence [in German]. Rofo 2002;174(1):70–75.
28. Chung YC, Merkle EM, Lewin JS, Shonk JR, Duerk JL. Fast T(2)-weighted imaging by PSIF at 0.2 T for interventional MRI. Magn Reson Med 1999; 42(2):335–344.
29. Boll DT, Lewin JS, Duerk JL, Aschoff AJ, Merkle EM. Comparison of MR imaging sequences for liver and head and neck interventions: is there a single optimal sequence for all purposes? Acad Radiol 2004;11(5):506–515.
30. Absil J, Denolin V, Metens T. Fat attenuation using a dual steady-state balanced-SSFP sequence with periodically variable flip angles. Magn Reson Med 2006;55:343–351.
31. So NM, Lam WW, Li D, et al. Magnetic resonance angiography of coronary arteries with a 3-dimensional magnetization-prepared true fast imaging with steady-state precession sequence compared with conventional coronary angiography. Am Heart J 2005;150(3):530–535.
32. Bi X, Deshpande V, Simonetti O, Laub G, Li D. Three-dimensional breathhold SSFP coronary MRA: a comparison between 1.5T and 3.0T. J Magn Reson Imaging 2005;22(2):206–212.
33. Keogan MT, Edelman RR. Technologic advances in abdominal MR imaging. Radiology 2001;220: 310–320.
34. Martin DR, Danrad R, Herrmann K, Semelka RC, Hussain SM. Magnetic resonance imaging of the gastrointestinal tract. Top Magn Reson Imaging 2005;16(1):77–98.
35. Chung HW, Chen CY, Zimmerman RA, et al. T2-weighted fast MR imaging with trueFISP versus HASTE: comparative efficacy in the evaluation of normal fetal brain maturation. AJR Am J Roentgenol 2000;175(5):1375–1380.
36. Ramli N, Cooper A, Jaspan T. High resolution CISS imaging of the spine. Br J Radiol 2001;74:862–873.
37. Yoshino N, Akimoto H, Yamada I, et al. Trigeminal neuralgia: evaluation of neuralgic manifestation and site of neurovascular compression with 3D CISS MR imaging and MR angiography. Radiology 2003;228:539–545.
38. Zausinger S, Yousry I, Bruceckmann, Schmid-Elaesser R, Tonn JC. Cavernous malformations of the brainstem: three-dimensional-constructive interference in steady-state magnetic resonance imaging for improvement of surgical approach and clinical results. Neurosurgery 2006;58(2):322–330.
39. van Ouwerkerk WJ, Strijers RL, Barkhof F, Umans U, Vandertop WP. Detection of root avulsion in the dominant C7 obstetric brachial plexus lesion: experience with three-dimensional constructive interference in steady-state magnetic resonance imaging and electrophysiology. Neurosurgery 2005;57(5): 930–940.
40. Jayakumar PN, Kovoor JM, Srikanth SG, Praharaj SS. 3D steady-state MR cisternography in CSF rhinorrhoea. Acta Radiol 2001;42(6):582–584.
41. Eckstein F, Hudelmaier M, Wirth W, et al. Double echo steady state magnetic resonance imaging of knee articular cartilage at 3 Tesla: a pilot study for the Osteoarthritis Initiative. Ann Rheum Dis 2006; 65(4):433–441.

Steady-State MR Imaging Sequences: Physics, Classification, and Clinical Applications

Govind B. Chavhan, MD, DNB, et al

RadioGraphics 2008; 28:1147–1160 • **Published online** 10.1148/rg.284075031 • **Content Codes:** MR PH

Page 1148
Note that although a GRE sequence with spoiled TM is not considered a classic steady-state sequence, steady state is achieved for the LM component. For this reason, these sequences have been called steady-state incoherent sequences by some authors (5). Classic steady-state sequences have been termed steady-state coherent sequences by these same authors (5).

Page 1149
FID (S+) has mixed T1 and T2* weighting. The spin echo (S[minus]) is strongly T2 weighted and has negligible T2* weighting.

Pages 1150
Depending on what signals are sampled and used for image formation, steady-state sequences can be classified as follows:

1. Postexcitation refocused steady-state sequences, in which only the FID (S+) component is sampled (eg, FISP [Siemens], GRASS [GE Medical Systems], FFE, Fourier-acquired steady-state technique [FAST; Picker International, Cleveland, Ohio]).
2. Preexcitation refocused steady-state sequences, in which only the spin-echo (S[minus]) component is used for image formation (eg, PSIF [reversed FISP, Siemens]; steady-state free precession [SSFP, GE Medical Systems]; T2-FFE).
3. Fully refocused steady-state sequences, in which both FID (S+) and spin-echo (S[minus]) components are used for image formation. This sequence is also called balanced SSFP, since gradients applied in all three axes are balanced (eg, true FISP, FIESTA [GE Medical Systems], balanced FFE).

Page 1152
The main difference between fully refocused steady-state sequences (balanced SSFP) and other GRE sequences is the use of balanced gradients in all three axes (slice-selection, phase-encoding, and readout) such that gradient-induced dephasing within TR is exactly zero. This makes balanced SSFP relatively insensitive to motion. In nonbalanced GRE sequences, slice-selection and readout gradients are not balanced.

Pages 1155
Contrast in balanced SSFP is dependent on the T2/T1 ratio. Blood has a much higher T2/T1 ratio than does myocardium. The sequence is flow compensated and intrinsically insensitive to flow because of even echo rephasing, which is due to the multiple GRE pulses used. An intrinsically high SNR makes it possible to image with a higher bandwidth and a very short TR. All of these factors make this sequence suitable for cardiac imaging.

RadioGraphics 2008

This is your reprint order form or pro forma invoice

(Please keep a copy of this document for your records.)

Reprint order forms and purchase orders or prepayments must be received 72 hours after receipt of form either by mail or by fax at 410-820-9765. It is the policy of Cadmus Reprints to issue one invoice per order. **Please print clearly**.

Author Name _____
Title of Article _____
Issue of Journal_____ Reprint # _____ Publication Date _____
Number of Pages_____ KB # _____ Symbol RadioGraphics
Color in Article? Yes / No (Please Circle)

Please include the journal name and reprint number or manuscript number on your purchase order or other correspondence.

Order and Shipping Information

Reprint Costs **(Please see page 2 of 2 for reprint costs/fees.)**

_____ Number of reprints ordered $_____
_____ Number of color reprints ordered $_____
_____ Number of covers ordered $_____
Subtotal $_____
Taxes $_____

(*Add appropriate sales tax for Virginia, Maryland, Pennsylvania, and the District of Columbia or Canadian GST to the reprints if your order is to be shipped to these locations*.)

First address included, add $32 for each additional shipping address $_____

TOTAL $_____

Shipping Address **(cannot ship to a P.O. Box) Please Print Clearly**

Name _____
Institution _____
Street _____
City _____ State _____ Zip _____
Country _____
Quantity_____ Fax _____
Phone: Day _____ Evening _____
E-mail Address _____

Additional Shipping Address* **(cannot ship to a P.O. Box)**

Name _____
Institution _____
Street _____
City _____ State _____ Zip _____
Country _____
Quantity _____ Fax _____
Phone: Day _____ Evening _____
E-mail Address _____

** Add $32 for each additional shipping address*

Payment and Credit Card Details

Enclosed: Personal Check _____
Credit Card Payment Details _____
Checks must be paid in U.S. dollars and drawn on a U.S. Bank.

Credit Card: __ VISA __ Am. Exp. __ MasterCard
Card Number _____
Expiration Date_____
Signature: _____

Please send your order form and prepayment made payable to:

Cadmus Reprints
P.O. Box 751903
Charlotte, NC 28275-1903

Note: Do not send express packages to this location, PO Box.
FEIN #:541274108

Invoice or Credit Card Information

Invoice Address Please Print Clearly
Please complete Invoice address as it appears on credit card statement

Name _____
Institution _____
Department _____
Street _____
City _____ State _____ Zip _____
Country _____
Phone _____ Fax _____
E-mail Address _____

Cadmus will process credit cards and *Cadmus Journal Services* will appear on the credit card statement.

If you don't mail your order form, you may fax it to 410-820-9765 with your credit card information.

Signature _____ Date _____

Signature is required. By signing this form, the author agrees to accept the responsibility for the payment of reprints and/or all charges described in this document.

RB-9/26/07

RadioGraphics 2008

Black and White Reprint Prices

Domestic (USA only)						
# of Pages	50	100	200	300	400	500
1-4	$221	$233	$268	$285	$303	$323
5-8	$355	$382	$432	$466	$510	$544
9-12	$466	$513	$595	$652	$714	$775
13-16	$576	$640	$749	$830	$912	$995
17-20	$694	$775	$906	$1,017	$1,117	$1,220
21-24	$809	$906	$1,071	$1,200	$1,321	$1,471
25-28	$928	$1,041	$1,242	$1,390	$1,544	$1,688
29-32	$1,042	$1,178	$1,403	$1,568	$1,751	$1,924
Covers	$97	$118	$215	$323	$442	$555

International (includes Canada and Mexico)						
# of Pages	50	100	200	300	400	500
1-4	$272	$283	$340	$397	$446	$506
5-8	$428	$455	$576	$675	$784	$884
9-12	$580	$626	$805	$964	$1,115	$1,278
13-16	$724	$786	$1,023	$1,232	$1,445	$1,652
17-20	$878	$958	$1,246	$1,520	$1,774	$2,030
21-24	$1,022	$1,119	$1,474	$1,795	$2,108	$2,426
25-28	$1,176	$1,291	$1,700	$2,070	$2,450	$2,813
29-32	$1,316	$1,452	$1,936	$2,355	$2,784	$3,209
Covers	$156	$176	$335	$525	$716	$905

Minimum order is 50 copies. For orders larger than 500 copies, please consult Cadmus Reprints at 800-407-9190.

Reprint Cover

Cover prices are listed above. The cover will include the publication title, article title, and author name in black.

Shipping

Shipping costs are included in the reprint prices. Domestic orders are shipped via UPS Ground service. Foreign orders are shipped via a proof of delivery air service.

Multiple Shipments

Orders can be shipped to more than one location. Please be aware that it will cost $32 for each additional location.

Delivery

Your order will be shipped within 2 weeks of the journal print date. Allow extra time for delivery.

Color Reprint Prices

Domestic (USA only)						
# of Pages	50	100	200	300	400	500
1-4	$223	$239	$352	$473	$597	$719
5-8	$349	$401	$601	$849	$1,099	$1,349
9-12	$486	$517	$852	$1,232	$1,609	$1,992
13-16	$615	$651	$1,105	$1,609	$2,117	$2,624
17-20	$759	$787	$1,357	$1,997	$2,626	$3,260
21-24	$897	$924	$1,611	$2,376	$3,135	$3,905
25-28	$1,033	$1,071	$1,873	$2,757	$3,650	$4,536
29-32	$1,175	$1,208	$2,122	$3,138	$4,162	$5,180
Covers	$97	$118	$215	$323	$442	$555

International (includes Canada and Mexico))						
# of Pages	50	100	200	300	400	500
1-4	$278	$290	$424	$586	$741	$904
5-8	$429	$472	$746	$1,058	$1,374	$1,690
9-12	$604	$629	$1,061	$1,545	$2,011	$2,494
13-16	$766	$797	$1,378	$2,013	$2,647	$3,280
17-20	$945	$972	$1,698	$2,499	$3,282	$4,069
21-24	$1,110	$1,139	$2,015	$2,970	$3,921	$4,873
25-28	$1,290	$1,321	$2,333	$3,437	$4,556	$5,661
29-32	$1,455	$1,482	$2,652	$3,924	$5,193	$6,462
Covers	$156	$176	$335	$525	$716	$905

Tax Due

Residents of Virginia, Maryland, Pennsylvania, and the District of Columbia are required to add the appropriate sales tax to each reprint order. For orders shipped to Canada, please add 7% Canadian GST unless exemption is claimed.

Ordering

Reprint order forms and purchase order or prepayment is required to process your order. Please reference journal name and reprint number or manuscript number on any correspondence. You may use the reverse side of this form as a proforma invoice. Please return your order form and prepayment to:

Cadmus Reprints
P.O. Box 751903
Charlotte, NC 28275-1903

Note: Do not send express packages to this location, PO Box.
FEIN #:541274108

Please direct all inquiries to:

Rose A. Baynard
800-407-9190 (toll free number)
410-819-3966 (direct number)
410-820-9765 (FAX number)
baynardr@cadmus.com (e-mail)

Reprint Order Forms and purchase order or prepayments must be received 72 hours after receipt of form.